

# Orientation dependent etching of silicon by fluorine molecules: a quantum chemistry computational study

Omesh Dhar Dwivedi <sup>1,2</sup>, Yuri Barsukov <sup>1,a</sup>, Sierra Jubin<sup>1,3</sup>, Joseph R. Vella<sup>1</sup>, and Igor Kaganovich<sup>1</sup>

<sup>1</sup>Princeton Plasma Physics Laboratory, Princeton University, Princeton, NJ, United States of America, 08543

<sup>2</sup>Drexel University, Philadelphia, PA, United States of America, 19104

<sup>3</sup>Princeton University, Princeton, NJ, United States, 08544

<sup>a)</sup> Electronic mail: [yvbarsuk@pppl.gov](mailto:yvbarsuk@pppl.gov)

Orientation-dependent etching is an interesting phenomenon which can be used for micro- and nano-scale texturing of silicon surfaces during black silicon production. We consider here the orientation-dependent plasma-less etching of silicon by molecular fluorine, which was previously established experimental. Moreover, this anisotropic process was implemented with atmospheric dry etching (ADE) technology. The nature of the anisotropy is that the etching in the (111) direction of the Si surface is significantly slower than that in the (100) and (110) directions. Using DFT (density functional theory) simulations, we performed quantum chemistry modelling of the reaction pathways determining the rates of the etching caused by F<sub>2</sub> dissociative chemisorption and subsequent Si-Si bond breaking. Dangling bonds on the surface Si atoms were passivated with fluorine. A charge density analysis indicates that F atoms attracts electron density from the Si atoms giving them a positive charge, whereas the neighboring Si atoms unpassivated with fluorine have a negative charge. The amount of positive charge increases with the number of F atoms bonded with silicon. Si(100) and Si(110) incorporate a larger number of fluorine atoms than Si(111) resulting in the Si-Si bonds on these surfaces have a larger amount of positive charge. The lower reaction barrier and higher etch rate of Si(100) and Si(110) compared to Si(111) is explained

by the fact that  $F_2$  molecule approaching the surface becomes negatively charged and more strongly attracts to the Si(100) and Si(110) surfaces than to the Si(111).

## I. INTRODUCTION

### A. *Silicon etching by molecular fluorine*

The orientation-dependent etching of silicon, in which the etch rate in the (111) direction is much slower than in the (100) and (110) directions, is a known phenomenon. It has been used for the texturing of silicon surfaces via dry and wet etching processes; this produces a product known as black silicon<sup>1,2</sup>. Plasma-less atmospheric dry etching (ADE) commercialized by Nines Photovoltaics is a cost-effective method of nano-scale silicon surface texturing. Namely, Kafle et al.<sup>3-6</sup> showed that at temperatures higher than 200  $^0C$ , textured surface with nano-scale pits are formed on an oxidized Si(100) surface during plasma-less etching by molecular fluorine gas diluted in  $N_2$  gas. Nucleation of the pits due to anisotropic etching start at reactive sites where the oxide layer is absence or have a pinhole. The slope of the pit walls is defined by the Si(111) surface, which intersects the Si(100) plane at an angle of about 55 degrees, as it is shown in Fig. 1. The cone-shaped nanostructures shown in Fig. 1b disappear with an increase in temperature beyond 300C (Fig. 1c) resulting in surface reflection increasing. The isotropic etching at high temperature can be explained by the fact that both the etch rate of Si(111) (see Section IIb and IV) and the degree of  $F_2$  dissociation increase with temperature. Thus, at high temperatures atomic fluorine rapidly etches silicon in all directions.

It should be note that a similar effect, where silicon is slowly etched in the (111) direction compared to the (100) direction by  $Cl_2/Ar$  inductively coupled plasma, was observed by Du et al.

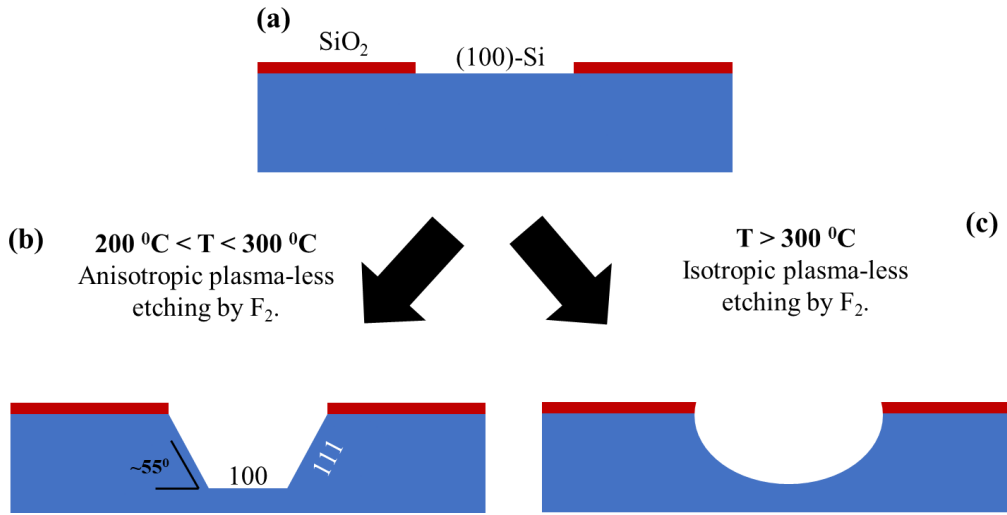


FIG. 1. Schematic representation of partly oxidized initial structure of Si(100) (a), the surface structure after the anisotropic (orientation-dependent) (b) and isotropic etching (c) by  $\text{F}_2$  molecules, which was observed by Kafle et al.<sup>3</sup>

Here we performed DFT (density function theory) simulations of reaction pathways of  $\text{F}_2$  dissociative chemisorption with subsequent Si-Si bond breaking, assuming that this is the rate limiting step of silicon etching by  $\text{F}_2$ . We showed that the activation barriers increase as follows: 0.13 eV on reconstructed Si(100), 0.31 eV on unreconstructed Si(100), 0.35 eV on Si(110) and 0.57 eV on Si(111). Note, that the structure of unreconstructed Si(100) does not differ from the structure of the silicon bulk, whereas surface atoms of a reconstructed Si(100) are shifted relative to their position in the bulk resulting surface free energy lowering<sup>8</sup>. We assume that the surface relaxation is a long process relative to the etching, therefore, the etching proceeds without the surface relaxation. Indeed, Mucha et al.<sup>9</sup> measured the rate of silicon etching by molecular fluorine, and found that it is given by the formula in Arrhenius form  $(3.94 \pm 0.65) \times 10^{-12} T^{1/2} \exp(-0.394 eV/kT)$ . This measurement yields both the rate of etching and the activation energy, and these values match the results of our quantum chemistry calculations of  $\text{F}_2$

chemisorption on the unreconstructed Si(100) and Si(110) (see Section IIB). This agreement with the etching experiment confirms our assumption that the etching rate is determined by the rate of  $F_2$  dissociative chemisorption on silicon surfaces.

Pullman et al.<sup>10</sup> experimentally studied the dissociative chemisorption of  $F_2$  on the Si(100)(2×1) surface saturated with a single monolayer of fluorine by exposing the fluorine-saturated surface to supersonic  $F_2$  beams of variable energy. They found that no reaction occurs below 0.16 eV of incident energy. Note that this experiment aimed to study the reaction of  $F_2$  dissociative chemisorption without subsequent etching. Therefore, we assume that the studied reaction proceeded on the initially relaxed Si(100). Indeed, the calculated here barrier of  $F_2$  dissociative chemisorption on reconstructed Si(100) surface (0.13 eV) is close to the measured threshold value of  $F_2$  incident energy (0.16 eV). In other words, we think that the measured threshold value of the  $F_2$  incident energy is determined by the barrier of  $F_2$  dissociative chemisorption.

The reaction of the Si(111) surface with molecular fluorine was studied by Tatsumi and Hiroi<sup>11</sup> in an ultra-high vacuum reactor. They found that the effective activation energy for the surface reactions of molecular fluorine leading to Si(111) surface etching at temperatures below 580 °C was 0.61 eV. According to our calculation the barrier of  $F_2$  dissociative chemisorption on Si(111) is 0.57 eV, which again confirms that  $F_2$  dissociative chemisorption determines the etch rate of silicon.

*Our DFT calculations reproduce the experimental trend that  $F_2$  more slowly reacts with the Si(111) surface relative to the other surface facets.. The charge density analysis under DFT approach showed that F atoms attracts electron density from the Si atom and the amount of positive charge on the Si atom increases with the number of F atoms bonded with Si. Si(100) and*

*Si(110) surfaces are passivated by a larger amount of F atoms compared to Si(111) as it is shown in Fig. 2. (The surface composition of Si(100) and Si(110) is Si:F = 1:1, while Si(111) is Si:F = 2:1). Thus, the amount of positive charge on Si-Si bonds of Si(100) and Si(110) surfaces is larger than the total positive charge on Si(111). F<sub>2</sub> molecules approaching the surface become negatively charged and, as a result, they are stronger attracted to Si(100) and Si(110) surfaces. As a result, the activation barrier ( $E_a$ ) during the etching is changed as follows:  $E_a$  (Si(100))  $\approx$   $E_a$  (Si(110)) <<  $E_a$  (Si(111)).*

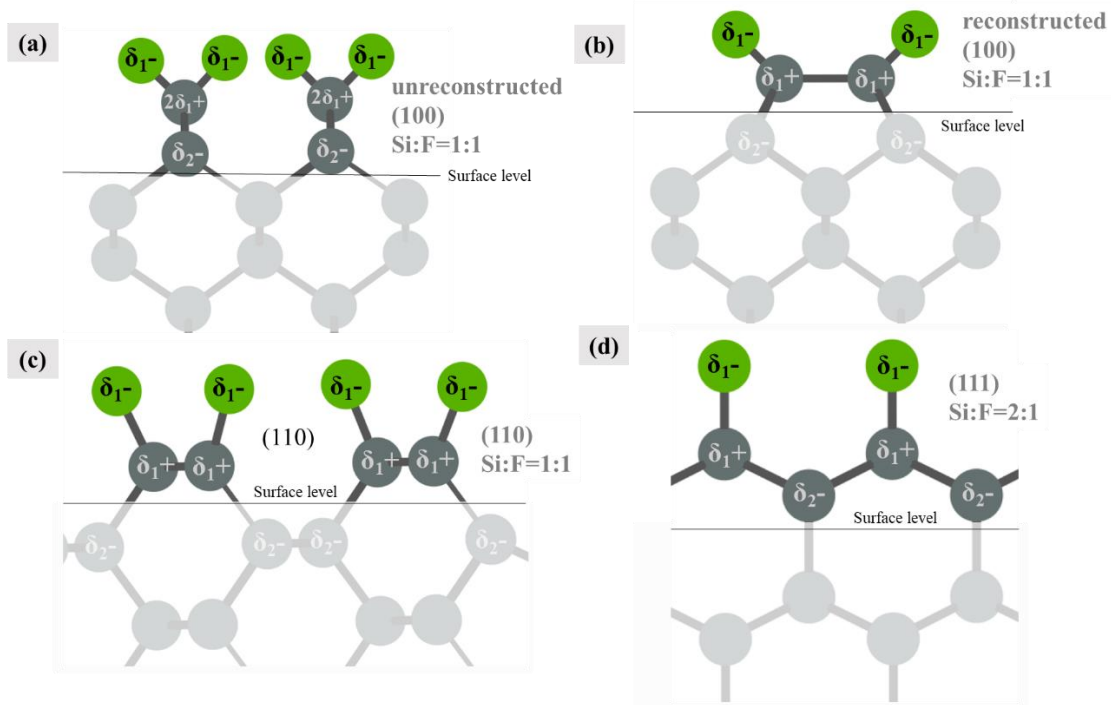


FIG. 2. Structure, composition and charge distribution of Si-Si bonds on unreconstructed Si(100) (a), reconstructed Si(100) (b), Si(110) (c), and Si(111) (d). Fluorine atoms are green cycles, silicon atoms are grey cycles.

## B. Silicon etching by other reagents

It should be noted that numerous reagents can be used for etching Si surfaces. Tajima et al.<sup>12,13</sup> studied the etching of Si surfaces using an F<sub>2</sub>/NO mixture, which produces F + FNO at an

elevated temperature. The purpose of using this reagent mixture stems from the fact that NO plays an important role in controlling F density. They studied the effect of the ratio of the individual components of the mixture and the effect of temperature on the surface morphology. They observed the formation of nano-porous features, and a crystallographically orientation-dependent etched profile when varying the temperature profile.

Arora et al.<sup>14</sup> found that the addition of SF<sub>6</sub> to NF<sub>3</sub> plasma mixtures led to an increased etch rate and left the substrate with smoother etched Si surfaces. They discuss the possible role of adsorbed S acting as a catalyst. In other studies, the effect of SF<sub>6</sub> on the surface morphologies of etched Si was also discussed<sup>15-17</sup>.

Chlorine-containing reagents for silicon etching have been studied in many publications. It was shown that HCl gas etches Si, SiGe and Ge at elevated temperatures<sup>18</sup>. Si etching requires temperatures above 750 °C, while Ge etching occurs above 350 °C. The etching of SiGe depends on the fractional Ge content in the film, and the activation barrier varies from 86.3 kcal/mol for silicon to 28.3 kcal/mol for pure germanium. In another study silicon was etched by a mixture of Cl<sub>2</sub> and F<sub>2</sub><sup>19</sup> which was burned to generate ClF molecules, the key reagent. The measured activation barrier for that etching process was found to be 19.8 kcal/mol. Silicon etching by ClF<sub>3</sub>, on the other hand, is temperature independent<sup>20</sup>, and the rate-limiting factor for that process is either the transport of ClF<sub>3</sub> through the reactor or diffusion of ClF<sub>3</sub> through the fluorinated surface layer<sup>21</sup>. For this type of etching, the shape of the profile (isotropic or anisotropic) depends on the size of the etched apertures. Etching based on atomic chlorine is also a widely studied method. It has been shown<sup>22-24</sup> that significant etching of Si by atomic chlorine can only take place at high temperatures. For example, the Si(100) etch rate is varied from 1 to 10 nm/min for temperatures ranging from 525 °C to 575 °C<sup>22</sup>. In this case, the dominant desorption products

are  $\text{SiCl}_4$  at  $T < 600 \text{ }^{\circ}\text{C}$  or  $\text{SiCl}_2$  at  $T > 500 \text{ }^{\circ}\text{C}$ . No atomic or molecular chlorine desorption is observed at  $T > 120 \text{ }^{\circ}\text{C}$ <sup>24</sup>. In addition, UV irradiation<sup>7,25</sup> and ion bombardment<sup>26,27</sup> drastically speed up the etching process.

Hydrogen-based etching of silicon is another interesting candidate investigated in many studies<sup>28–36</sup>. Veprek et al.<sup>29</sup> found that in pure hydrogen glow discharge plasmas, the etch rate of Si shows an Arrhenius-like dependence on temperature: as temperature increases, the etching rate also increases up to a certain temperature, at which point the trend reverses and the etching rate decreases with increasing temperature. The etching remains anisotropic within all studied conditions. Later Veprek et al.<sup>30</sup> showed that oxygen impurities cause an adverse effect on the etching rate with complete termination of Si etching by atomic hydrogen for impurities beyond the 70 ppm mark.

## II. QUANTUM CHEMISTRY MODELLING

### A. *Computational details*

Quantum chemistry modelling was performed using broken symmetry orbitals calculated by the unrestricted u-B3LYP DFT functional in the Gaussian 16<sup>37</sup> software package. Lanl2dz basis set and pseudopotential for Si atoms were used in our simulations.

A  $\text{Si}_{32}\text{F}_{32}$  cluster (Fig. 3) was used to mimic the structure of fluorinated Si surfaces. The free bonds of external Si atoms were closed by fluorine atoms. The geometries of four transition states (TSs) corresponding to the reactions of  $\text{F}_2$  dissociative chemisorption on a Si(100) surface with and without surface reconstruction, on a Si(110) surface, and on a Si(111) surface are shown in Fig. 3. In all transition states considered here the F-F bond is perpendicular to the Si-Si bonds. On the reaction path after the transition state, an intermediate bi-radical structure is

observed where singlet and triplet states are overlapping, as shown in Fig. 4. Natural population analysis was performed to calculate atomic charges from Fig. 4, which can be found Table 1, where  $\delta_{1\text{Si}}^{\text{Si}}$  and  $\delta_{2\text{Si}}^{\text{Si}}$  are atomic charges on Si atoms,  $\delta^{\text{Si}2}$  and  $\delta^{\text{F}2}$  are charges on  $\text{Si}_2$  and  $\text{F}_2$  dimers in transition state.

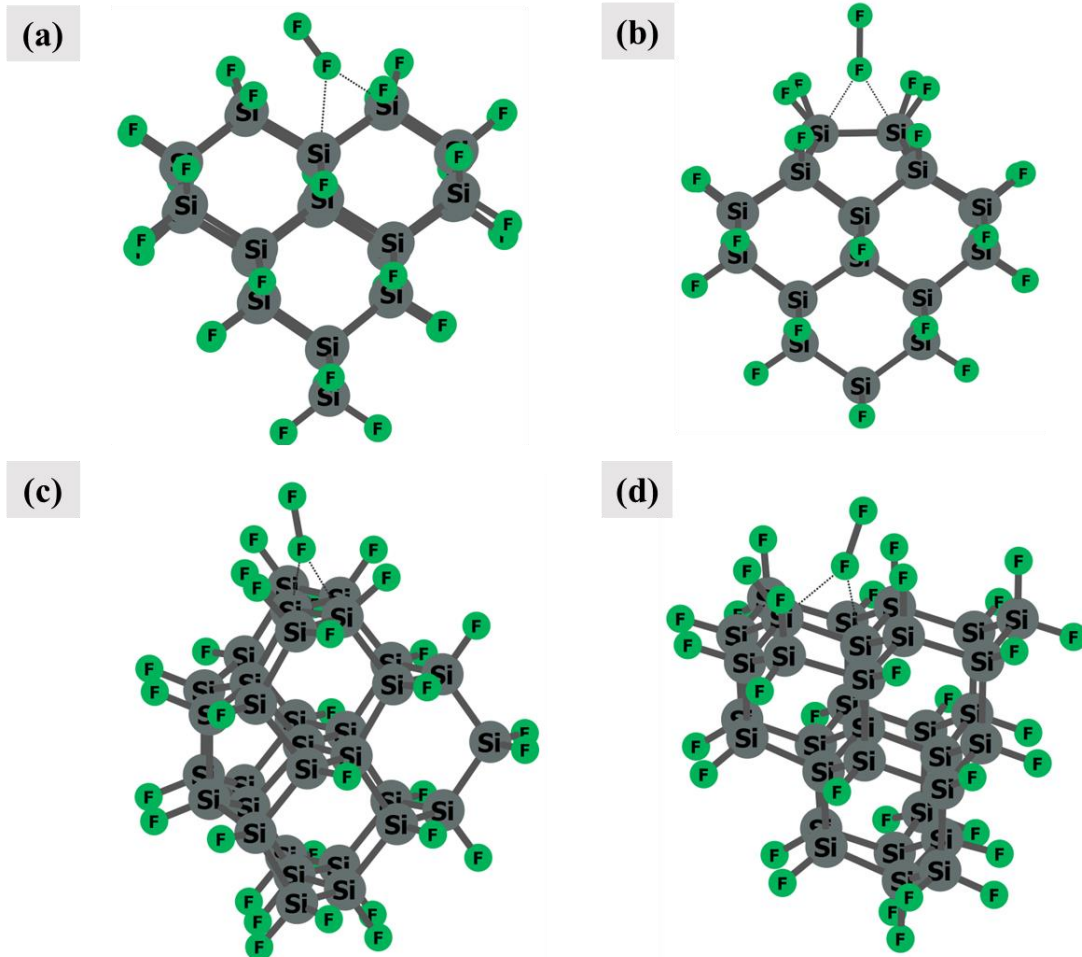


FIG. 3. Geometries of transition states of  $\text{F}_2$  dissociative chemisorption on unreconstructed  $\text{Si}(100)$  (a), reconstructed  $\text{Si}(100)$  (b),  $\text{Si}(110)$  (c) and  $\text{Si}(111)$  (d) surface of  $\text{Si}_{32}\text{F}_{32}$  cluster.

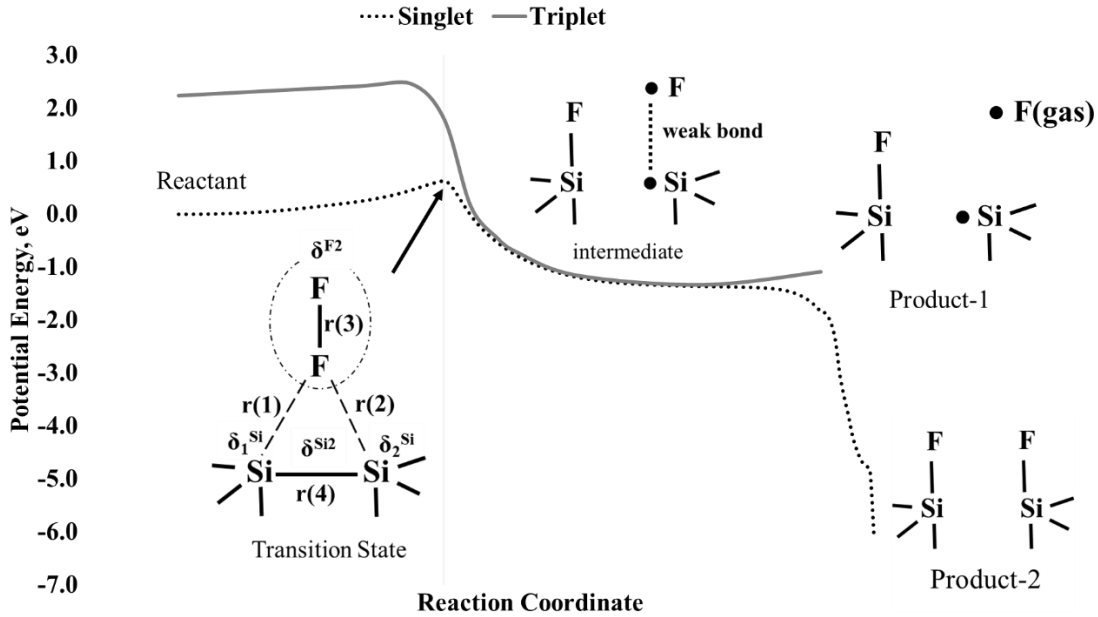


FIG. 4. Reaction pathway of  $\text{F}_2$  dissociative chemisorption on a 111-oriented surface of  $\text{Si}_{32}\text{F}_{32}$  cluster. The structures of transition state and products are schematically shown, where  $r(1)$ ,  $r(2)$ ,  $r(3)$  and  $r(4)$  are distances;  $\delta_1^{\text{Si}}$  and  $\delta_2^{\text{Si}}$  are charges on the attacked Si atoms,  $\delta^{\text{Si}2}$  and  $\delta^{\text{F}2}$  is the total charge on the attacked Si-Si bonds and attacking  $\text{F}_2$  molecule (See Table 1).

Pre-exponential factors in the Arrhenius equations were calculated using the Eyring equation <sup>38</sup>:

$$A = \frac{k_B T}{h} \frac{Z_{vib}^{TS}}{Z_{vib}^{Si32F32} Z_{tot}^{F2}} \quad (1)$$

where  $k_B$  and  $h$  are Boltzmann's and Planck's constants,  $Z_{vib}^{TS}$  and  $Z_{vib}^{Si32F32}$  are vibrational partition functions of the TS geometry and the isolated  $\text{Si}_{32}\text{F}_{32}$  cluster, and  $Z_{tot}^{F2}$  is the total partition function of the isolated  $\text{F}_2$  molecule. The partition functions in eq(1) were calculated using Gaussian 16 software. The pre-exponential factor  $A$  in eq(1) is a function of temperature, therefore it was fitted using the standard form in a temperature range from 298.15 to 1000K:

$$A = A'(T/298.15)^{n1} \quad (2)$$

The rate of the surface reaction can be described either as a reaction probability or in standard Arrhenius form:

$$\frac{1}{4} \gamma \sqrt{\frac{8k_B T}{\pi m}} C_{F2} = \frac{k_B T}{h} \frac{Z_{vib}^{TS}}{Z_{vib}^{Si32F32} Z_{tot}^{F2}} \exp\left(-\frac{Ea}{k_B T}\right) \rho_s C_{F2} \quad (3)$$

where  $m$  and  $C_{F2}$  are the mass and density of  $F_2$ ,  $E_a$  is the activation energy of the reaction and  $\rho_s$  is the surface site density. Thus, the probability  $\gamma$  of  $F_2$  dissociative chemisorption can be calculated using the next equation:

$$\gamma(T) = \gamma_0(T) \sqrt{\frac{T}{T_0}} \exp\left(-\frac{Ea}{k_B T}\right) = \gamma'_0 \left(\frac{T}{T_0}\right)^{n2} \exp\left(-\frac{Ea}{k_B T}\right) \quad (4)$$

where  $\gamma_0(T) = \frac{\sqrt{2\pi m k_B}}{h} \frac{Z_{vib}^{TS}}{Z_{vib}^{Si32F32} Z_{tot}^{F2}} \rho_s \sqrt{T_0}$  depends on temperature, because the partition functions are functions of temperature. Hereinafter we will assume that  $T_0 = 298.15$  K.  $\gamma'_0 \left(\frac{T}{T_0}\right)^{n2}$  is a function, where  $\gamma'_0$  and  $n2$  parameters were chosen to fit calculated  $\gamma_0(T) \sqrt{\frac{T}{T_0}}$  values at a temperature range from 298.15 to 1000K. The values of  $E_a$ ,  $\gamma'_0$ ,  $n1$  and  $n2$  can be found in Table 2, where these parameters are substituted into the expression of rate constants and probabilities:

$$k(T) = A_0 \left(\frac{T}{298.15}\right)^{n1} \exp\left(-\frac{Ea}{k_B T}\right) \quad (5a)$$

$$\gamma(T) = \gamma'_0 \left(\frac{T}{298.15}\right)^{n2} \exp\left(-\frac{Ea}{k_B T}\right) \quad (5b)$$

## B. DFT validation

We studied  $F_2$  dissociative chemisorption on different sides of the  $Si_{32}F_{32}$  cluster, which mimic fluorinated  $Si(100)$ ,  $Si(110)$ , and  $Si(111)$  surfaces. Transition states are presented in Fig. 3. The reaction pathway of  $F_2$  dissociation on the (111)-oriented surface is shown in Fig. 4 as an example. The presence of the biradical structure is consistent with dissociative chemisorption via single atom abstraction as proposed by Tate et al.<sup>39,40</sup>, in which only one atom of  $F_2$  forms a  $Si-F$

bond while the other F atom desorbs into gas phase (product-1 in Fig. 4). The product-2 in Fig. 4 corresponds to the reaction channel of dissociative chemisorption, where both atoms of the F<sub>2</sub> molecule adsorb on the silicon surface resulting in two Si-F bonds. Note that molecular dynamic simulations by Carter et al. <sup>41</sup> showed that both reaction channels yielding product-1 and product-2 are present and they are the dominant reaction channels on a clean unpassivated by fluorine Si(100) surface. *We expect that the reaction channel with single atom abstraction decreases the selectivity of orientation-dependent etching because the desorbed F atom non-selectively etches Si(100), Si(110) and Si(111) surfaces.*

As mentioned in the introduction, Mucha et al. measured the rate of silicon etching by F<sub>2</sub> gas. Unfortunately, they did not mention the orientation of the silicon surface exposed to the reactants. Nevertheless, we can compare our etching rate constant ( $R$ ) calculated using equation (6) with the measured  $R$  by Mucha et al. (Section II A).

$$R = A * \left( \frac{T}{298.15} \right)^n * \exp \left( -\frac{E_a}{RT} \right) * \frac{M(Si)}{p(Si) * N_A}, \quad (6)$$

$$Etch\ Rate = R * n_{F2}, \quad (7)$$

where  $M(Si)$  is the molar mass of silicon,  $p(Si)$  is the density of bulk silicon,  $N_A$  is Avogadro's number, and  $A$  and  $E_a$  are the pre-exponential factor and activation energy of F<sub>2</sub> dissociative chemisorption on a Si<sub>32</sub>F<sub>32</sub> cluster (Section II A).

The results are presented in Fig. 5, which shows that our calculations give good agreement with experimental data if we assume that the surface orientation in the experiment was Si(100) or Si(110).

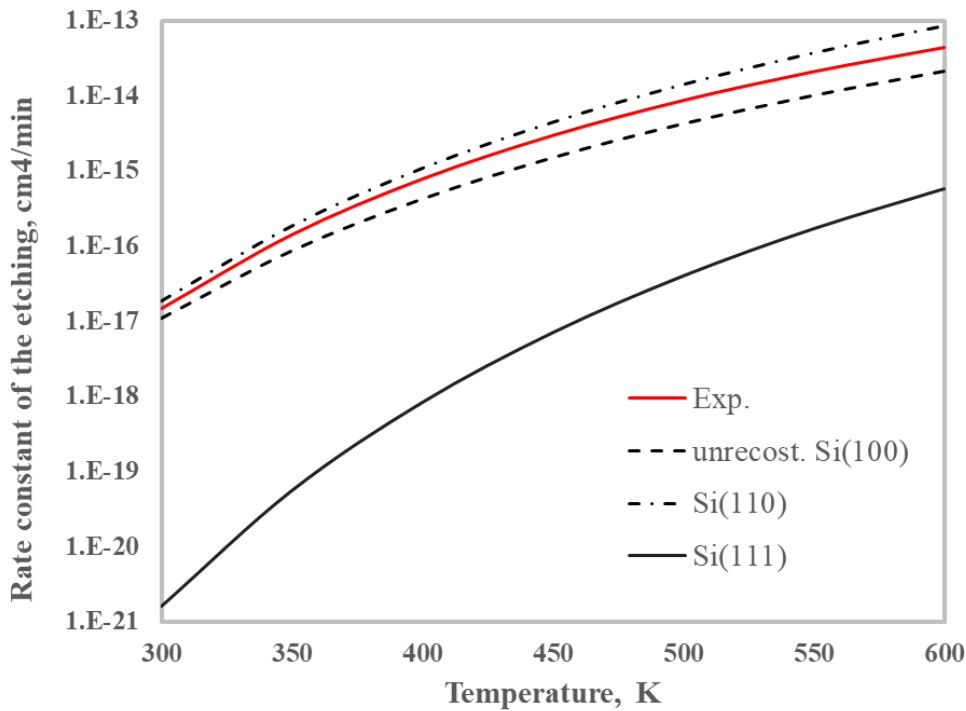


FIG. 5. Calculated rate constants of  $\text{F}_2$  dissociative chemisorption on unreconstructed  $\text{Si}(100)$ ,  $\text{Si}(110)$  and  $\text{Si}(111)$  surfaces by  $\text{F}_2$  in  $\text{cm}^4/\text{min}$ , compared to measured etching rate constant by Mucha et al <sup>9</sup> in solid red.

Thus, our modelling qualitatively describes the dissociative chemisorption mechanism. At the same time, our modelling accurately reproduces experimental values of the etching rate for Si etching by molecular  $\text{F}_2$ .

### III. Classical Molecular Dynamics

We also performed classical molecular dynamics (MD) simulations to deepen our understanding of the crystal facet dependent etching of Si by  $\text{F}_2$ . In these simulations, Si-F interactions are described using a reactive empirical bond order (REBO) potential. These types of force fields are commonly used to simulate covalently bonded materials (such as Si), as well

as their reactions with a variety of gaseous species. We use the REBO potential parameterized by Humbird and Graves<sup>42</sup>.

In order to utilize the MD code in an efficient manner, we simulate the etching process by a series of “impact simulations”. These simulations consist of a semi-infinite Si slab with a vacuum space above the slab in the  $z$  direction. The Si slab consists of Si atoms in a diamond-cubic lattice. Periodic boundary conditions are imposed in the  $x$  and  $y$  directions to make the slab semi-infinite. The bottom two layers are fixed to prevent drift of the slab due to incoming  $F_2$  impacts. During an “impact simulation” a  $F_2$  molecule is placed in a random position in the vacuum space above the Si slab. The height of the molecule is chosen such that it is just outside the interaction distance of the Si slab. The velocity components of the  $F_2$  are randomly sampled from the Maxwell-Boltzmann distribution at 300 K. We only consider molecules with a negative  $z$  component of velocity, so the molecule will impact the Si slab. Next, a microcanonical ensemble (constant number of atoms, constant volume, and constant total energy), MD simulation is run lasting approximately 2 ps. After the trajectory is complete, species that have been etched or sputtered are deleted from the simulation. Species that are also weakly bound to the surface are also deleted. After this, a Berendsen thermostat<sup>43</sup> is applied to the simulation cell to remove excess energy introduced by the incoming species, and to maintain the temperature of the Si slab. More information on the thermostat procedure and product deletion routines can be found in previous work<sup>26,44</sup>. This procedure is repeated until the desired fluence of  $F_2$  is reached. We consider Si slabs with different crystal facets facing the vacuum space to study the different etching behavior of the facets. The surface area for the Si slab with the (100) surface exposed (both unreconstructed and reconstructed) is about  $472.5 \text{ \AA}^2$ . For the slab with the (110) surface exposed, the surface area is about  $626.4 \text{ \AA}^2$ . The surface area for the Si slab with the (111)

surface exposed is roughly  $613.8 \text{ \AA}^2$ . The depth of each cell is large enough such that no  $\text{F}_2$  molecules will interact with the fixed layer. The lattice constant in all cells corresponds to diamond cubic Si at 300 K. Even though we consider temperatures higher than 300 K, the lattice constant remains the same in our simulations. In reality, the crystal will expand as temperature is raised. However, because the thermal expansion of Si is very small (the lattice constant increases by about 0.5% from 298.5 K to 1513.2 K<sup>45</sup>) we ignore this expansion in our simulations.

Our classical MD simulations did not show a silicon etching at temperature below 900 K ( $\text{F}_2$  bounced off from the silicon surfaces every time). In order to explain the absence of the etching we performed DFT calculations of intrinsic reaction coordinate (IRC) of  $\text{F}_2$  dissociative chemisorption on  $\text{Si}_{32}$  cluster for all TSs shown in Fig3. IRC is the steepest descent path from TS to the reagent and product valleys. The same reaction pathways were recalculated by the REBO classical MD potential. As it is shown in Fig. 6(a), (b) and (c), the very high barriers appear on the (100) and (110) reactions paths recalculated by the classical MD potential, while the (111) reaction path is quite accurately reproduced by REBO potential. Thus, no etching by REBO potential at T below 900 K can be explained by the fact that, due to the high reaction barriers, the reactions are very slow below 900 K and, as a result, they cannot be simulated by classical MD in a reasonable amount of time. In the case of (100) and (110) surfaces the barriers are overestimated and additional fitting of the potential would be required for  $\text{Si} + \text{F}_2$  chemistry in order to correct this. The (111) barrier calculated by the REBO potential is very close to the DFT value (0.61 eV vs. 0.57 eV), but the reaction is still longer than 1 ns at T below 900 K (see Fig. 6(d)). The etching probabilities calculated by classical MD and probabilities of  $\text{F}_2$  dissociative chemisorption calculated by transition state theory can be found in Fig. 7.

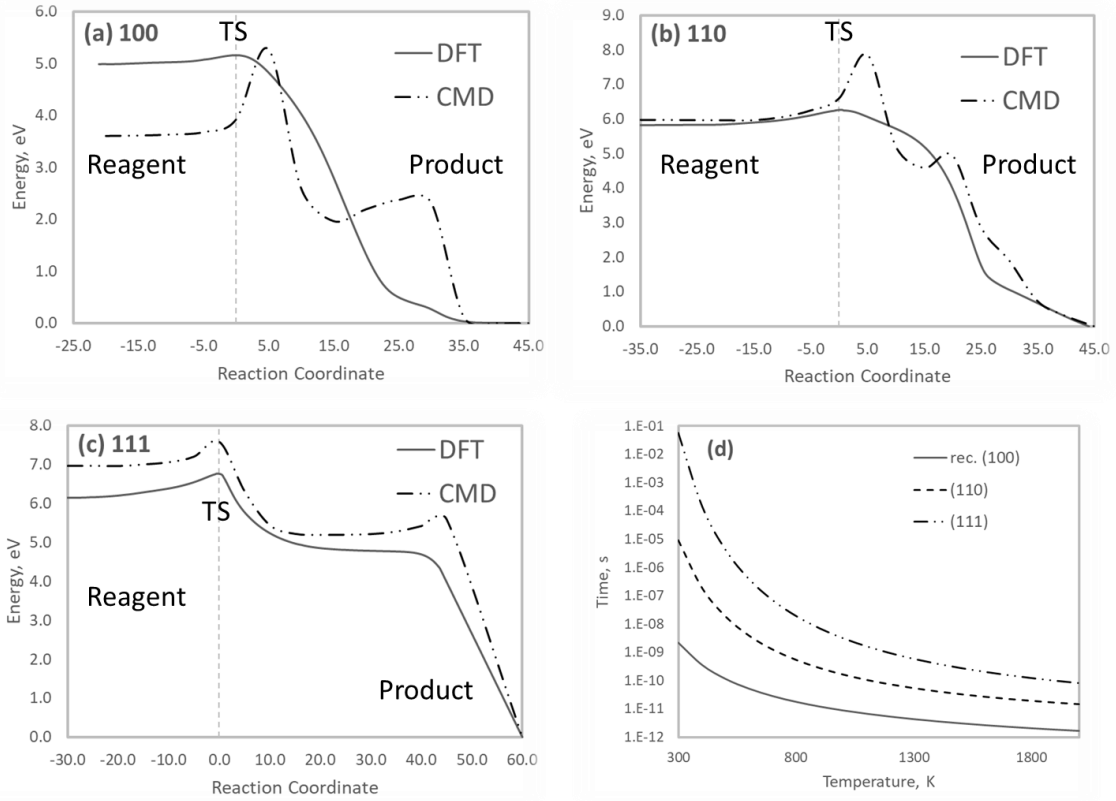


FIG. 6. Reaction path of  $\text{F}_2$  dissociative chemisorption on reconstructed (100) (a), (110) (b) and (111) (c) surfaces of  $\text{Si}_{32}$  cluster calculated by DFT and recalculated with the REBO classical MD (CMD) potential. Time of these reactions was calculated by DFT (d).

## IV. RESULTS AND DISCUSSION

As our simulation shows, the dissociative chemisorption of  $\text{F}_2$  on  $\text{Si}(111)$  proceeds over a significantly higher barrier than dissociative chemisorption on  $\text{Si}(100)$  and  $\text{Si}(110)$  surfaces. This results in a lower reaction probability (Fig. 7) and hence a lower etch rate for the  $\text{Si}(111)$  surface. We also demonstrate that etching of the (100) surface with reconstruction is faster than etching on the (100) surface without reconstruction. We assume that the reconstruction takes a longer time than etching, therefore the removal of surface layers by fluorine proceeds without the

reconstruction. It is equally probable that the  $F_2$  molecule dissociates on unreconstructed (100) and (110) surfaces (Fig. 7) and, as a result, the etching in (100) and (110) directions proceeds with the same rate. The low etch rate of the Si(111) surface by comparison explains orientation-dependent etching of silicon, which was used by Kafle et al.<sup>3–6</sup> for texturing silicon surfaces during black silicon production.

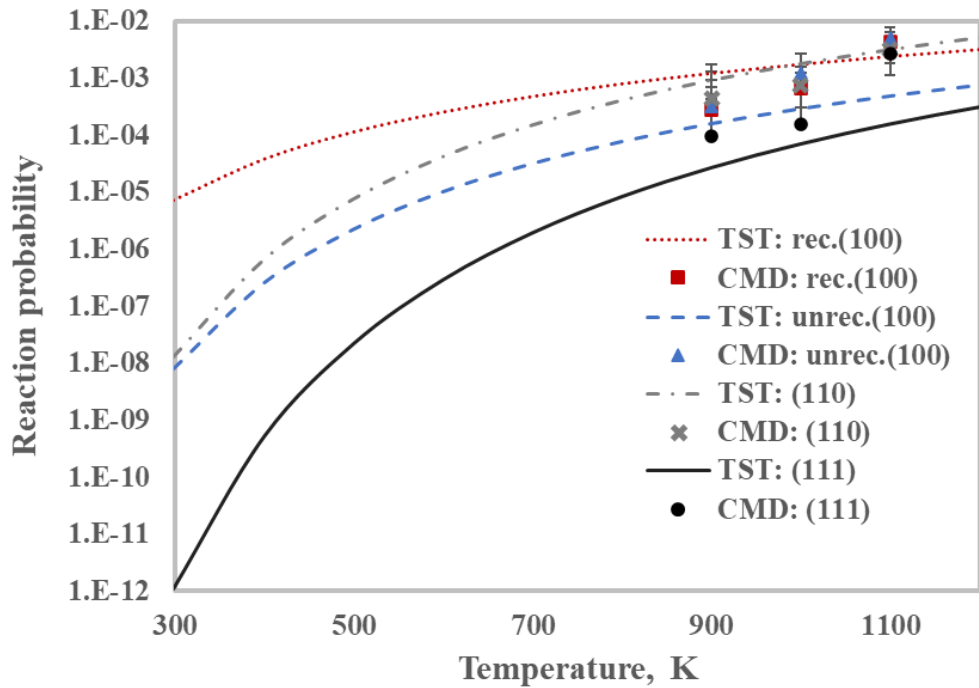


FIG. 7. The probabilities of  $F_2$  dissociative chemisorption on a  $Si_{32}F_{32}$  cluster calculated by transition state theory (TST) under DFT approach and probabilities of the silicon slab etching calculated by classical MD (CMD) for (100), (110) and (111) silicon surfaces.

We attribute the high etch rate of Si(100) and Si(110) to the fact that these surfaces incorporates a large number of F atoms resulting amount of positive charge on Si-Si bonds is larger. Indeed, the positive charge on the attacked Si-Si bond  $\delta^{Si2}$  (see Table 1) decreases as follows: reconstructed (100) > unreconstructed (100)  $\approx$  (110) > (111).  $F_2$  molecule approaching

to the surface becomes negatively charged (Table 1) and stronger attracts to the Si-Si bonds on Si(100) and Si(110) resulting in lower activation barrier of the  $F_2$  chemisorption (Table 2).

As it was mentioned in Section IIB, one of the possible reaction channels is  $F_2$  dissociative chemisorption via single atom abstraction, in which one of F atoms of attacking  $F_2$  molecule desorbs into the gas phase. The desorbed F atom can secondarily react with silicon surface and equiprobable break Si-Si bonds on Si(100), Si(110) and Si(111) resulting in isotropic etching.

Finally, we collect calculated parameters for rate constants and probabilities of  $F_2$  dissociative chemisorption on silicon surfaces in Table 2.

TABLE I. Geometric and electronic characteristics of transition states for the reactions of  $F_2$  dissociative chemisorption on the (100), (110) and (111) surfaces of a  $Si_{32}F_{32}$  cluster.  $r(1)$ ,  $r(2)$ ,  $r(3)$  and  $r(4)$  are distances;  $\delta_1$  and  $\delta_2$  are charges on the Si atoms of the attacked dimer, and  $\delta_3$  is the total charge on the  $F_2$  molecule (see Fig. 2). 100a and 100b indicate the (100) surface with reconstruction and without reconstruction, respectively.

Surface	$r(1)$ , Å	$r(2)$ , Å	$r(3)$ , Å	$r(4)$ , Å	$\delta_1^{Si}$	$\delta_2^{Si}$	$\delta^{Si2}$	$\delta^{F2}$
rec.100	2.49	2.49	1.56	2.57	+0.79	+0.79	+1.58	-0.17
unrec.100	2.17	2.43	1.60	2.54	-0.25	+1.55	+1.30	-0.24
110	2.28	2.42	1.59	2.51	+0.73	+0.63	+1.36	-0.22
111	2.35	2.34	1.60	2.62	-0.26	+0.79	+0.56	-0.22

TABLE 2. Rate constants and probabilities of  $F_2$  dissociative chemisorption on the (100), (110) and (111) surfaces of a  $Si_{32}F_{32}$  cluster. The rate constants and the probabilities are expressed in Arrhenius form according to equations 5a and 5b.  $E_a^{exp}$  is the experimental value of the

activation energy. Rec. 100 and unrec. 100 indicate the (100) surface with reconstruction and without reconstruction, respectively.

Surface	$A^{\wedge}$ , m <sup>3</sup> /s	$n1$	$\gamma_0^{\wedge}$	$n2$	$E_a$ , eV	$E_a^{exp}$ , eV
rec.100	$8.82 \cdot 10^{-21}$	2.20	0.0011	1.60	0.13	$0.16^{10}$
unrec.100	$1.23 \cdot 10^{-20}$	2.20	0.0016	1.70	0.31	$0.39^9$
110	$7.52 \cdot 10^{-20}$	2.50	0.0096	1.96	0.35	
111	$3.90 \cdot 10^{-20}$	2.50	0.0050	1.96	0.57	$0.61^{11}$

## V. CONCLUSION

Orientation-dependent etching of silicon via molecular  $F_2$  has been studied using quantum chemistry methods. Activation barriers, reaction rates, and probabilities for  $F_2$  dissociative chemisorption on (100), (110) and (111) surfaces were calculated. It was shown that the barrier of  $F_2$  dissociative chemisorption on Si(111) is significantly higher than on (100) and (110) surfaces. Natural population analysis showed that partial negative charge accumulates on the  $F_2$  molecule and also on half of the Si atoms of (111)-oriented surfaces. As a result, an additional repulsive force appears between molecular  $F_2$  and Si(111) surfaces. This explains why the calculated probability of  $F_2$  dissociative chemisorption on the Si(111) is significantly lower than on Si(100) and Si(110). Our simulation results are consistent with previously published experimental data and explain the mechanism of orientation-dependent etching of Si by  $F_2$  gas. According to our data the activation barrier of  $F_2$  dissociative chemisorption depends on amount of positive charge on the attacked Si-Si bond on the fluorinated silicon surface.

Additionally, we describe the presence of a biradical plateau on the potential energy surface of  $F_2$  dissociative chemisorption. We expect that the desorption of F atoms from the

biradical structure is significant during the etching process. This is consistent with dissociative chemisorption via single atom abstraction, which was proposed previously. We expect that the reaction channel via single atom abstraction will decrease orientation-dependent etching selectivity.

## REFERENCES

- (1) Hsu, C.-H.; Wu, J.-R.; Lu, Y.-T.; Flood, D. J.; Barron, A. R.; Chen, L.-C. Fabrication and Characteristics of Black Silicon for Solar Cell Applications: An Overview. *Materials Science in Semiconductor Processing* **2014**, *25*, 2–17. <https://doi.org/10.1016/j.mssp.2014.02.005>.
- (2) H Jansen; M de Boer; R Legtenberg; M Elwenspoek. The Black Silicon Method: A Universal Method for Determining the Parameter Setting of a Fluorine-Based Reactive Ion Etcher in Deep Silicon Trench Etching with Profile Control. *Journal of Micromechanics and Microengineering* **1995**, *5* (2), 115. <https://doi.org/10.1088/0960-1317/5/2/015>.
- (3) Kafle, B.; Ridoy, A. I.; Miethig, E.; Clochard, L.; Duffy, E.; Hofmann, M.; Rentsch, J. On the Formation of Black Silicon Features by Plasma-Less Etching of Silicon in Molecular Fluorine Gas. *Nanomaterials* **2020**, *10* (11). <https://doi.org/10.3390/nano10112214>.
- (4) Kafle, B.; Ridoy, A. I.; Saint-Cast, P.; Clochard, L.; Duffy, E.; Duncker, K.; Petter, K.; Hofmann, M.; Rentsch, J. Atmospheric Pressure Dry Texturing Enabling 20% Conversion Efficiency on Multicrystalline Silicon PERC Solar Cells; Lausanne, Switzerland, 2018; p 050003. <https://doi.org/10.1063/1.5049293>.
- (5) Kafle, B.; Seiffe, J.; Hofmann, M.; Clochard, L.; Duffy, E.; Rentsch, J. Nanostructuring of C-Si Surface by F<sub>2</sub>-Based Atmospheric Pressure Dry Texturing Process. *Phys. Status Solidi A* **2015**, *212* (2), 307–311. <https://doi.org/10.1002/pssa.201431372>.
- (6) Kafle, B.; Freund, T.; Mannan, A.; Clochard, L.; Duffy, E.; Werner, S.; Saint-Cast, P.; Hofmann, M.; Rentsch, J.; Preu, R. Plasma-Free Dry-Chemical Texturing Process for High-Efficiency Multicrystalline Silicon Solar Cells. *Energy Procedia* **2016**, *92*, 359–368. <https://doi.org/10.1016/j.egypro.2016.07.113>.
- (7) Du, L.; Economou, D. J.; Donnelly, V. M. In-Plasma Photo-Assisted Etching of Si with Chlorine Aided by an External Vacuum Ultraviolet Source. *Journal of Vacuum Science & Technology B* **2022**, *40* (2), 022207. <https://doi.org/10.1116/6.0001710>.
- (8) Ramstad, A.; Brocks, G.; Kelly, P. J. Theoretical Study of the Si(100) Surface Reconstruction. *Phys. Rev. B* **1995**, *51* (20), 14504–14523. <https://doi.org/10.1103/PhysRevB.51.14504>.
- (9) Mucha, J. A.; Donnelly, V. M.; Flamm, D. L.; Webb, L. M. Chemiluminescence and the Reaction of Molecular Fluorine with Silicon. *J. Phys. Chem.* **1981**, *85* (23), 3529–3532. <https://doi.org/10.1021/j150623a032>.
- (10) Pullman, D. P.; Tsekouras, A. A.; Li, Y. L.; Yang, J. J.; Tate, M. R.; Gosalvez, D. B.; Laughlin, K. B.; Schulberg, M. T.; Ceyer, S. T. Reactivity of Fluorinated Si(100) with F<sub>2</sub>. *J. Phys. Chem. B* **2001**, *105* (2), 486–496. <https://doi.org/10.1021/jp002443v>.

- (11) Masayuki Hiroi, M. H.; Toru Tatsumi, T. T. Temperature Dependence of Etching with Molecular Fluorine on Si(111) Surface. *Japanese Journal of Applied Physics* **1994**, *33* (4S), 2244. <https://doi.org/10.1143/JJAP.33.2244>.
- (12) Tajima, S.; Hayashi, T.; Ishikawa, K.; Sekine, M.; Hori, M. Room-Temperature Si Etching in NO/F<sub>2</sub> Gases and the Investigation of Surface Reaction Mechanisms. *J. Phys. Chem. C* **2013**, *117* (10), 5118–5125. <https://doi.org/10.1021/jp3119132>.
- (13) Tajima, S.; Hayashi, T.; Ishikawa, K.; Sekine, M.; Hori, M. Formation of Nanoporous Features, Flat Surfaces, or Crystallographically Oriented Etched Profiles by the Si Chemical Dry Etching Using the Reaction of F<sub>2</sub> + NO → F + FNO at an Elevated Temperature. *J. Phys. Chem. C* **2013**, *117* (40), 20810–20818. <https://doi.org/10.1021/jp4084794>.
- (14) Priyanka Arora; Nguyen, T.; Chawla, A.; Nam, S.-K.; Donnelly, V. M. Role of Sulfur in Catalyzing Fluorine Atom Fast Etching of Silicon with Smooth Surface Morphology. *Journal of Vacuum Science & Technology A* **2019**, *37* (6), 061303. <https://doi.org/10.1116/1.5125266>.
- (15) Hays, D. C.; Jung, K. B.; Hahn, Y. B.; Lambers, E. S.; Pearton, S. J.; Donahue, J.; Johnson, D.; Shul, R. J. Comparison of F<sub>2</sub>-Based Gases for High-Rate Dry Etching of Si. *Journal of The Electrochemical Society* **1999**, *146* (10), 3812. <https://doi.org/10.1149/1.1392556>.
- (16) Belen, R. J.; Gomez, S.; Kiehlbauch, M.; Cooperberg, D.; Aydil, E. S. Feature-Scale Model of Si Etching in SF<sub>6</sub> Plasma and Comparison with Experiments. *Journal of Vacuum Science & Technology A* **2005**, *23* (1), 99–113. <https://doi.org/10.1116/1.1830495>.
- (17) Herrick, A.; Perry, A. J.; Boswell, R. W. Etching Silicon by SF<sub>6</sub> in a Continuous and Pulsed Power Helicon Reactor. *Journal of Vacuum Science & Technology A* **2003**, *21* (4), 955–966. <https://doi.org/10.1116/1.1575215>.
- (18) Bogumilowicz, Y.; Hartmann, J. M.; Truche, R.; Campidelli, Y.; Rolland, G.; Billon, T. Chemical Vapour Etching of Si, SiGe and Ge with HCl; Applications to the Formation of Thin Relaxed SiGe Buffers and to the Revelation of Threading Dislocations. *Semiconductor Science and Technology* **2004**, *20* (2), 127. <https://doi.org/10.1088/0268-1242/20/2/004>.
- (19) Fletcher, E. A.; Dahneke, B. E. Kinetics of the Chlorine Fluoride Reaction. *J. Am. Chem. Soc.* **1969**, *91* (7), 1603–1608. <https://doi.org/10.1021/ja01035a004>.
- (20) Habuka, H.; Sukenobu, T.; Koda, H.; Takeuchi, T.; Aihara, M. Silicon Etch Rate Using Chlorine Trifluoride. *Journal of The Electrochemical Society* **2004**, *151* (11), G783. <https://doi.org/10.1149/1.1806391>.
- (21) Höchst, A.; Fischer, F.; Kirbach, G.; Urban, A.; Becker, V.; Irmscher, M.; Sailer, H.; Kern, D. P. Investigations on the Mechanism of Silicon Etching with Chlorine-Trifluoride. *Journal of Vacuum Science & Technology B: Microelectronics and Nanometer Structures Processing, Measurement, and Phenomena* **2005**, *23* (5), 1936–1942. <https://doi.org/10.1116/1.2013313>.
- (22) Chung, K. H.; Sturm, J. C. Chlorine Etching for In-Situ Low-Temperature Silicon Surface Cleaning for Epitaxy Applications. *ECS Transactions* **2007**, *6* (1), 401. <https://doi.org/10.1149/1.2727426>.
- (23) Violette, K. E.; O’Neil, P. A.; Öztürk, M. C.; Christensen, K.; Maher, D. M. On the Role of Chlorine in Selective Silicon Epitaxy by Chemical Vapor Deposition. *Journal of The Electrochemical Society* **1996**, *143* (10), 3290. <https://doi.org/10.1149/1.1837200>.

- (24) Szabó, A.; Farrall, P. D.; Engel, T. Reactions of Chlorine with Si(100) and Si(111): Adsorption and Desorption Kinetics. *Surface Science* **1994**, *312* (3), 284–300. [https://doi.org/10.1016/0039-6028\(94\)90722-6](https://doi.org/10.1016/0039-6028(94)90722-6).
- (25) Samukawa, S.; Jinnai, B.; Oda, F.; Morimoto, Y. Surface Reaction Enhancement by UV Irradiation during Si Etching Process with Chlorine Atom Beam. *Japanese Journal of Applied Physics* **2007**, *46* (1L), L64. <https://doi.org/10.1143/JJAP.46.L64>.
- (26) Vella, J. R.; Graves, D. B. Modification of a Force Field for Molecular Dynamics Simulations of Silicon Etching by Chlorine Atoms. *Journal of Vacuum Science & Technology A* **2022**, *40* (6), 063203. <https://doi.org/10.1116/6.0002027>.
- (27) Matsuura, T.; Murota, J.; Sawada, Y.; Ohmi, T. Self-limited Layer-by-layer Etching of Si by Alternated Chlorine Adsorption and Ar+ Ion Irradiation. *Appl. Phys. Lett.* **1993**, *63* (20), 2803–2805. <https://doi.org/10.1063/1.110340>.
- (28) Thedjoisworo, B. A.; Cheung, D.; Zamani, D. Characterization of Hydrogen–Plasma Interactions with Photoresist, Silicon, and Silicon Nitride Surfaces. *Journal of Vacuum Science & Technology A* **2012**, *30* (3), 031303. <https://doi.org/10.1116/1.4705512>.
- (29) Vepřek, S.; Sarott, F.-A. Electron-Impact-Induced Anisotropic Etching of Silicon by Hydrogen. *Plasma Chemistry and Plasma Processing* **1982**, *2* (3), 233–246. <https://doi.org/10.1007/BF00566522>.
- (30) Veprek, S.; Wang, C.; Veprek-Heijman, M. G. J. Role of Oxygen Impurities in Etching of Silicon by Atomic Hydrogen. *Journal of Vacuum Science & Technology A* **2008**, *26* (3), 313–320. <https://doi.org/10.1116/1.2884731>.
- (31) Bianco, G. V.; Losurdo, M.; Giangregorio, M. M.; Capezzuto, P.; Bruno, G. Real Time Monitoring of the Interaction of Si (100) with Atomic Hydrogen: The “H-Insertion/Si-Etching” Kinetic Model Explaining Si Surface Modifications. *Appl. Phys. Lett.* **2009**, *95* (16), 161501. <https://doi.org/10.1063/1.3245312>.
- (32) Otobe, M.; Kimura, M.; Oda, S. Selective Etching of Hydrogenated Amorphous Silicon by Hydrogen Plasma. *Japanese Journal of Applied Physics* **1994**, *33* (7S), 4442. <https://doi.org/10.1143/JJAP.33.4442>.
- (33) Hiraoka, Y. S. Elementary Processes of Si(001) Etching by Atomic Hydrogen. *Japanese Journal of Applied Physics* **2002**, *41* (2R), 784. <https://doi.org/10.1143/JJAP.41.784>.
- (34) H N Wanka; M B Schubert. High Silicon Etch Rates by Hot Filament Generated Atomic Hydrogen. *Journal of Physics D: Applied Physics* **1997**, *30* (8), L28. <https://doi.org/10.1088/0022-3727/30/8/002>.
- (35) Sato, T.; Sugiura, T.; Ohtsubo, M.; Matsuno, S.; Konagai, M. Texture Etching of Si with Atomic Hydrogen Generated by Hot Wire Method through SiO<sub>2</sub> Masks for Solar Cell Applications. *Japanese Journal of Applied Physics* **2007**, *46* (10R), 6796. <https://doi.org/10.1143/JJAP.46.6796>.
- (36) Wanka, H. N.; Schubert, M. B. Fast Etching of Amorphous and Microcrystalline Silicon by Hot-Filament Generated Atomic Hydrogen. *MRS Proceedings* **1997**, *467*, 651. <https://doi.org/10.1557/PROC-467-651>.
- (37) M. J. Frisch, G. W. Trucks, H. B. Schlegel, G. E. Scuseria,; M. A. Robb, J. R. Cheeseman, G. Scalmani, V. Barone,; G. A. Petersson, H. Nakatsuji, X. Li, M. Caricato, A. V. Marenich,; J. Bloino, B. G. Janesko, R. Gomperts, B. Mennucci, H. P. Hratchian,; J. V. Ortiz, A. F. Izmaylov, J. L. Sonnenberg, D. Williams-Young,; F. Ding, F. Lipparini, F. Egidi, J. Goings, B. Peng, A. Petrone,; T. Henderson, D. Ranasinghe, V. G. Zakrzewski, J. Gao, N. Rega,; G. Zheng, W. Liang, M. Hada, M. Ehara, K. Toyota, R. Fukuda,; J.

- Hasegawa, M. Ishida, T. Nakajima, Y. Honda, O. Kitao, H. Nakai,; T. Vreven, K. Throssell, J. A. Montgomery, Jr., J. E. Peralta,; F. Ogliaro, M. J. Bearpark, J. J. Heyd, E. N. Brothers, K. N. Kudin,; V. N. Staroverov, T. A. Keith, R. Kobayashi, J. Normand,; K. Raghavachari, A. P. Rendell, J. C. Burant, S. S. Iyengar,; J. Tomasi, M. Cossi, J. M. Millam, M. Klene, C. Adamo, R. Cammi,; J. W. Ochterski, R. L. Martin, K. Morokuma, O. Farkas,; J. B. Foresman, and D. J. Fox. Gaussian 16, 2016.
- (38) Eyring, H. The Activated Complex in Chemical Reactions. *J. Chem. Phys.* **1935**, *3* (2), 107–115. <https://doi.org/10.1063/1.1749604>.
- (39) Tate, M. R.; Gosalvez-Blanco, D.; Pullman, D. P.; Tsekouras, A. A.; Li, Y. L.; Yang, J. J.; Laughlin, K. B.; Eckman, S. C.; Bertino, M. F.; Ceyer, S. T. Fluorine Atom Abstraction by Si(100). I. Experimental. *J. Chem. Phys.* **1999**, *111* (8), 3679–3695. <https://doi.org/10.1063/1.479677>.
- (40) Tate, M. R.; Pullman, D. P.; Li, Y. L.; Gosalvez-Blanco, D.; Tsekouras, A. A.; Ceyer, S. T. Fluorine Atom Abstraction by Si(100) II. Model. *J. Chem. Phys.* **2000**, *112* (11), 5190–5204. <https://doi.org/10.1063/1.481092>.
- (41) Carter, L. E.; Khodabandeh, S.; Weakliem, P. C.; Carter, E. A. First-principles-derived Dynamics of F<sub>2</sub> Reactive Scattering on Si(100)-2×1. *The Journal of Chemical Physics* **1994**, *100* (3), 2277–2288. <https://doi.org/10.1063/1.466526>.
- (42) Humbird, D.; Graves, D. B. Improved Interatomic Potentials for Silicon–Fluorine and Silicon–Chlorine. *The Journal of Chemical Physics* **2004**, *120* (5), 2405–2412. <https://doi.org/10.1063/1.1636722>.
- (43) Berendsen, H. J. C.; Postma, J. P. M.; Van Gunsteren, W. F.; DiNola, A.; Haak, J. R. Molecular Dynamics with Coupling to an External Bath. *The Journal of Chemical Physics* **1984**, *81* (8), 3684–3690. <https://doi.org/10.1063/1.448118>.
- (44) Humbird, D. W. Computational Studies of Plasma-Surface Interactions, University of California, Berkeley, CA, 2004.
- (45) Okada, Y.; Tokumaru, Y. Precise Determination of Lattice Parameter and Thermal Expansion Coefficient of Silicon between 300 and 1500 K. *Journal of Applied Physics* **1984**, *56* (2), 314–320. <https://doi.org/10.1063/1.333965>.